A Theoretical Study of an Integrated Quantum-Well Resonant Tunneling Oscillator Initiated by an IMPATT Diode

Cheng Chih Yang *Member, IEEE* and Dee-Son Pan, *Member, IEEE*

***Abstract*— A novel initiation scheme, utilizing the new pulsed IMPATT to generate millimeter-wave oscillations in a series-integrated quantum-well resonant tunneling diode (RTD), is proposed and theoretically investigated for the first time. To facilitate transient analysis, a generalized impedance is defined and adopted in this work. The detailed investigation of a two-RTD oscillator is carried out at 100 GHz. The maximum oscillator output power versus the minimum initial input power required of initiation is about 50%. The duration of only a few RF cycles is needed for such initiation.**

I. Introduction

THE quantum-well resonant tunneling diode (RTD) has been very attractive in the past few years for its potential as a millimeter-wave oscillator [1], [2]. Currently, oscillations up to 712 GHz have been achieved [3]. The power generation capabilities can be enhanced by a series integration of RTD's. The RF performance of the series-integrated RTD devices used as high-frequency oscillators through a shock-wave stabilization scheme, which was demonstrated in series-connected tunnel diodes [4], has been recently investigated by us [5]. In this scheme, a sufficiently fast switch to turn on a dc power supply in a picosecond range is needed in order to initiate a millimeter-wave oscillation for the series-integrated RTD. The previously developed GaAs nonlinear transmission line (NLTL), which can generate voltage shock waves in about a picosecond [6], was selected as a fast switch in our investigations in [5].

In this paper, an alternative initiation scheme, which utilizes the recently reported new pulsed IMPATT diode [7] to generate millimeter-wave oscillation in the series-integrated quantum-well RTD device, is proposed and theoretically investigated for the first time. It has been demonstrated that a new pulsed operation mode of the IMPATT diode can deliver more than 50-W peak output power with 10% conversion efficiency under low duty cycle in the 94-GHz window [7]. This new mode [7] utilizes space-charge induced impact ionization throughout the device active region to shape the device current for high output power and efficiency. Therefore, it is bound to operate in a very short pulse due to inevitable thermal effect. It is possible to operate this IMPATT mode at even higher frequencies such as beyond 400 GHz, so is our initiated oscillation scheme. Since individual quantum-well RTD, independent of space charge effect, produces higher efficiency than IMPATT [8], it can be operated at relatively lower current density. Therefore, the series-integrated RTD oscillator can be operated in CW mode without thermal problem. However, it is well known that such series integration is dc unstable. As will be shown, the proposed RF initiation scheme can solve the instability problem by utilizing a pulsed source such as the new IMPATT mode.

To be specific, a reflection-type circuitry employing a circulator will be analyzed. To facilitate analysis, we have adopted and generalized the treatments of IMPATT oscillators and amplifiers derived by Kurokawa [9] and Kuno [10]. The interactions between device and circuit in the case of series-integrated RTD become more complicated. In this work, we have defined a generalized impedance to simplify the transient analysis. Shown in Fig. 1 is a simplified circulator-coupled circuit schematic, consisting of a circulator, an impedance transformer, a tuning element, and a two-terminal active device. The RF equivalent circuit model of a two-terminal active device is assumed to be a capacitance in shunt with a nonlinear negative conductance. The tuning element is basically an inductance for phase adjustment. Because a large device area can provide more output power, a small load resistance (less than 50 Ω) is preferred. Therefore, a transformer, which can be a quarter-wavelength section, is utilized for impedance transformation. Fig. 1 will serve as our basic circuit configuration for the formulation and analysis throughout this paper. The circuit configuration is suitable for quasi-optical application as well. The basic idea behind the proposed scheme is briefly presented in the following.

For a single RTD, the circuit operation is very similar to that of an IMPATT, except the dc bias is voltage-controlled. For a series-integrated quantum-well RTD device, the total output power will increase approximately by a factor of n^2, where n is the number of the integrated RTD's. However, from previous investigations, a stable negative conductance does not exist in the series-integrated RTD device if the total RF voltage amplitude across the device is less than a cutoff value (V_c) [5]. At V_c the integrated device usually exhibits the maximum stable negative conductance [5]. Due to the dc instability associated with the series-integrated RTD device,

Manuscript received March 1, 1993; revised March 2, 1994. This work was supported by the Air Force Office of Scientific Research under contract F49620-92-C-0055.

C. C. Yang is with TRW Inc., Space & Electronics Group, Redondo Beach, CA 90278 USA.

D.-S. Pan is with the Electrical Engineering Department, University of California, Los Angeles, CA 90024 USA.

IEEE Log Number 9406827.

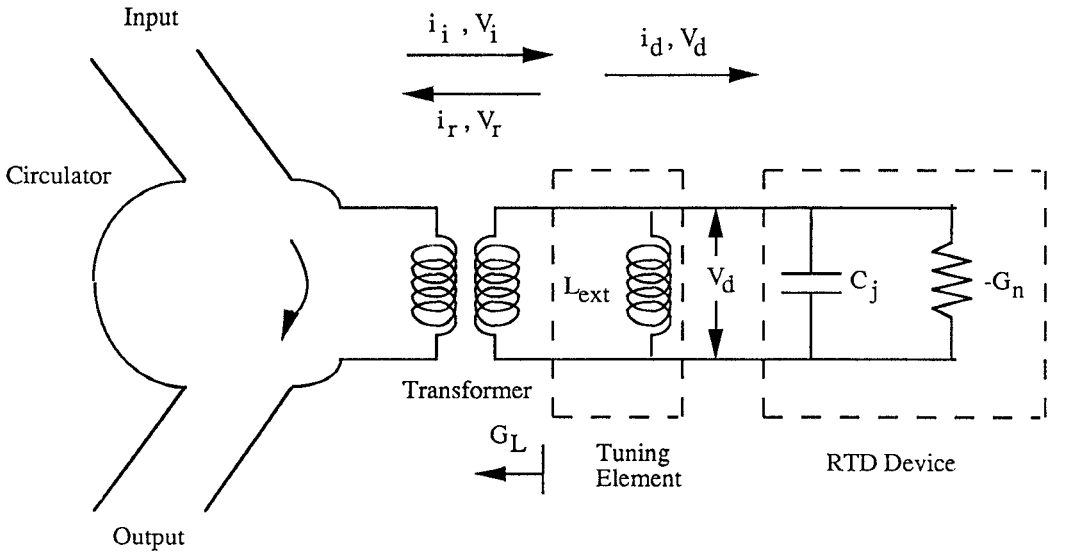

Fig. 1. A simplified circulator-coupled RTD circuit model used for circuit analysis.

the initial dc bias voltage across each individual RTD is always in the positive differential resistance (PDR) region of its I-V curve [5]. There also exists a RF threshold voltage (V_t), below which the dc operating point of each individual RTD cannot be switched from the PDR region into the NDR region [11]. Usually V_t is greater than V_c, and the absolute value of the device negative conductance at V_t is smaller.

Based on our theoretical analysis and simulation results, we find that the total RF voltage amplitude from the initiation pulse across the integrated device must be no less than V_t in order to relocate the dc bias point of each RTD into the NDR region. After dc bias point of each RTD is changed into NDR region by the RF pulse, the total device conductance changes from positive to negative value. The device conductance, whose value is determined by the load conductance, will be stabilized as the amplitude of the RF pulse voltage diminishes. Before the steady-state oscillator mode is reached, the circuit is in an amplifier mode. The transition from the amplifier mode to the oscillator mode is through an injection lock-in mode. The maximum power generated by the series-integrated RTD oscillator occurs when the load conductance is matched to the maximum of the device steady-state negative conductance. As will be shown later, the maximum output power versus the minimum initiation input power is about 50%, and only few RF cycles are required. That is to say, to generate a certain CW power, only twice of the power in a very short pulse is needed to initiate the oscillation.

A complete simulation of a two-RTD oscillator is carried out at 100 GHz to demonstrate that the proposed initiation approach is viable in the millimeter- and submillimeter-wave frequencies. The analysis technique can also be applied to a n-RTD oscillator. A GaAs/AlAs quantum-well RTD in [12] and its relevant parameters are adopted in the simulation. The circulator-coupled circuit model will be formulated in Section II. The interactions between the matching circuit and the active device are derived in Section III, where transient analysis is presented by utilizing the generalized impedance. Section IV shows an analytical solution to the oscillator circuit. Section V presents the simulation results. Finally, we conclude our investigation in Section VI.

II. Circuit Model Formulation

Kurokawa's model in [9] analyzed a circulator-coupled two-terminal oscillator circuit in great detail. On the other hand, the circuit equations derived by Kuno in [10] were formulated for circulator-coupled IMPATT amplifiers. For the series-integrated quantum-well RTD the general relationship between device conductance and amplitude of the RF voltage across the device is much more complicated than the IMPATT [5]. The equations in [10] cannot be applied directly. Therefore, in this section we would briefly present our derivation required for the circuit analysis. The derivation procedure is very similar to that presented in [9]. For the convenience of comparing the amplifier analysis by Kuno in [10], we have adopted admittance in our formulation instead of impedance as was done by Kurokawa [9]. However, it will be shown that the equations derived by us can be reduced to those in [10] if the device conductance of [10] is used.

For a single value of the terminal voltage across a series-integrated device structure, there are a number of different ways to partition this voltage across each individual RTD. The terminal current in the integrated device depends on the previous history of the terminal voltage and current for more than a period of the fundamental frequency. This complicated situation has not been systematically solved to our knowledge. To simplify the analysis, we have further generalized the impedance concept from the well-defined steady-state situation to an instantaneous quantity determined by one period of the fundamental frequency. Then, the problem associated with the interaction between the device and the circuit has to be treated in an interactive fashion.

We assume that the RF voltage across a two-terminal diode is a quasi-periodic function of time with a fundamental carrier frequency f ($= \omega/2\pi$), and that the higher harmonic components of the RF voltage are small enough to be ignored.

$$V(t) = \mathrm{Re}\left[V_o A(t) e^{j(\omega t + \jmath(t))}\right] \tag{1}$$

where V_o is an arbitrary nonzero constant. $A(t)$ and $\varphi(t)$ are amplitude- and phase-modulation functions, respectively [10]. $A(t)$ and $\varphi(t)$ are assumed to be relatively slow functions of time in comparison with the carrier frequency, therefore, $d\varphi/dt$ and $(1/A)(dA/dt)$ are small compared to ω.

The generalized admittance of the diode $(-Y_n)$ can be expressed as

$$-Y_n(A,\omega) = -G_n(A,\omega) + jB_n(A,\omega) \tag{2}$$

Notice that $Y_n(A,\omega), G_n(A,\omega)$, and $B_n(A,\omega)$ are functions of amplitude $A(t)$ and fundamental carrier frequency. They are defined as the instantaneous parameters at the instant t by calculating the Fourier components of the voltage and current waveforms determined by only one RF period, ending at t, of the fundamental frequency. The t dependence of Y_n, G_n, and B_n are through the function $A(t)$, which is a functional relationship. To a good approximation, the net current flowing through the diode is

$$\begin{aligned} i_d(t) = &\operatorname{Re}\left[-Y_n(A,\omega)V_o A(t)e^{j(\omega t+\varphi(t))}\right] \\ &+ (\text{harmonic components}) \end{aligned} \tag{3}$$

The harmonic components in current are not ignored, as done in [9]. The load circuit admittance (Y_L) seen by the diode is given as

$$Y_L(\omega) = G_L(\omega) + jB_L(\omega) \tag{4}$$

The corresponding current flowing through the load circuit is

$$\begin{aligned} i_L(t) = &\operatorname{Re}\left[Y_L(\omega)V_o A(t)e^{j(\omega t+\varphi(t))}\right] \\ &+ (\text{harmonic components}) \end{aligned} \tag{5}$$

To facilitate the derivation, a current source (i_s) is assumed and expressed as

$$i_s(t) = i_d(t) + i_L(t) \tag{6}$$

To obtain equations for A and φ, we follow a well-known procedure for nonlinear analysis [9]. We get

$$\begin{aligned} \operatorname{Re}\{&[-Y_n(A,\omega + d\varphi/dt - j(1/A)(dA/dt)) \\ &+ Y_L(\omega + d\varphi/dt - j(1/A)(dA/dt))]A\} = i_{sc}(t) \end{aligned} \tag{7}$$

$$\begin{aligned} -\operatorname{Im}\{&[-Y_n(A,\omega + d\varphi/dt - j(1/A)(dA/dt)) \\ &+ Y_L(\omega + d\varphi/dt - j(1/A)(dA/dt))]A\} = i_{ss}(t) \end{aligned} \tag{8}$$

where

$$i_{sc}(t) = \frac{2}{T}\int_{t-T}^{t} i_s(t)\cos(\omega_t + \varphi)\,dt \tag{9}$$

$$i_{ss}(t) = \frac{2}{T}\int_{t-T}^{t} i_s(t)\sin(\omega_t + \varphi)\,dt, \tag{10}$$

and Re and Im stand for real and imaginary parts, respectively. T is one RF period.

i_s in (9) and (10) is undetermined, but can be realized by employing the traveling wave concept as was done in [10]. As shown in Fig. 1, the voltage and the current components of the incident and the reflected waves are represented by V_i, i_i, V_r, and i_r, where the subscripts stand for incident and reflected, respectively. The net current flowing into the diode (i_d) and voltage across the diode (V_d) are given as

$$i_d = i_i - i_r \tag{11}$$

$$V_d = V_i + V_r \tag{12}$$

All the voltage components have the same form as (1). After a simple manipulation, i_s has a following form

$$i_s = \operatorname{Re}\left[2Y_L(\omega)V_o A_i(t)e^{j(\omega t+\varphi_i(t))}\right] \tag{13}$$

where A_i and φ_i are amplitude and phase of the input voltage wave, respectively.

To compare Kuno's equations, we adopt the equivalent circuit model of the IMPATT as described in [10]. Equation (2) and (4) become

$$-Y_n = (-g_n + \gamma V_d^2) + j[\omega C_j - 1/\omega(1/L_{\text{ext}} + 1/l_a + \lambda V_d^2)] \tag{14}$$

$$Y_L = G_L \tag{15}$$

where $-g_n$ and l_a are small-signal parameters, and γ, λ, and C_j are constants. Substituting (13)–(15) into (7) and (8), and keeping only terms involving the fundamental frequency, e.g., $\cos^3\phi \approx 3/4\cos\phi$, we can obtain a set of nonlinear coupled differential equations which are the same as (17) and (18) in [10].

For simplicity the RF circuit model of the active series-integrated quantum-well RTD device shown in Fig. 1 is assumed to be composed of a depletion capacitance (C_j) in shunt with a negative conductance $(-G_n)$. C_j is approximately a constant, and its value depends upon the number of the integrated RTD's and the total device area. The small nonlinearity in C_j will generate harmonics, which are expected to be insignificant. G_n is afunction of V_d and ω, and yet to be determined. The parasitic series resistance is not explicitly shown in the RF circuit model, because it is already lumped into G_n. (14) is then simplified to

$$-Y_n = -G_n(V_d,\omega) + j[\omega C_j - 1/\omega(1/L_{\text{ext}})] \tag{16}$$

Using (15) and (16), we obtain

$$\begin{aligned} &(2/\omega_o)\,dA_d/dt + [G_L - G_n(A_d,\varphi_d,\omega)]/(\omega_o C_j)A_d \\ &\quad = \eta A_i\cos(\varphi_i - jd) \end{aligned} \tag{17}$$

$$(2/\omega_o)A_d\,d\varphi_d/dt + \delta A_d = \eta A_i\sin(\varphi_i - \varphi_d) \tag{18}$$

where

$$\begin{aligned} \delta &\approx (2/\omega_o)(\omega - \omega_o) \\ \eta &= 2G_L/(\omega_o C_j) \\ \omega_o^2 &= 1/(L_{\text{ext}}C_j) \end{aligned} \tag{19}$$

Notice that $G_n'(A_d,\omega) = 0$ is assumed in the derivation, where prime represents the derivative with respect to ω. This means that device conductance has a certain frequency bandwidth at RF voltage amplitude of A_d. The operating frequency (ω)

has also been assumed to be close to the resonance frequency (ω_o). The voltage wave across the device generally includes both amplitude and phase, G_n in (17) is thus added a phase dependence term. The transit time effects are not implicitly included in G_n of (17) because of the complexities. Indeed, the RF performance degradation due to transit time effects can be estimated to be unimportant at this frequency [5], [13].

III. Circuit and Device Interactions

The circulator-coupled series-integrated RTD circuit is governed by (17) and (18), which have two unknowns, i.e., A_d and φ_d, to be solved. Unfortunately, G_n in (17) is a nonlinear function of A_d and φ_d, and impossible to be expressed explicitly in terms of A_d and φ_d. This really complicates the numerical solution process. Therefore, we would briefly describe the numerical simulation mechanism involving circuit and device interactions.

When a RF power is injected at input port of the circulator, it can be treated as an incident traveling wave. As mentioned earlier, the incident wave instantaneously sees different device impedance due to the history of the RF voltage amplitude variation across the device. The total dc voltage across the device is intended to bias every individual RTD near the center voltage point of the NDR region. The net device conductance starts with a positive value, because dc bias of each individual RTD is located in the PDR regions when power supply is slowly turned on. As the amplitude of the total RF voltage across the device, which is the sum of the incident and the reflected waves, is increased, dc bias point of each RTD will gradually move towards NDR region. Eventually, all the dc bias points will be pulled into NDR region as long as the total RF voltage amplitude across the device is greater than V_t [11]. Two sets of nonlinear coupled differential equations are involved in the transient solution process. The first set determines the transient conductance of the series-integrated quantum-well RTD device. The resulting instantaneous conductance ($G_n(t)$) will plug into the second set of nonlinear coupled differential equations to solve transient amplitude ($A_d(t)$) and phase ($\varphi_d(t)$) of the total RF voltage across the device. These instantaneous transient parameters will continue varying with time until a stabilized steady state is reached.

The numerical simulation algorithm is explained in detail by a flow chart illustrated in Fig. 2. The amplitude (A_i) and phase (φ_i) of the incident sinusoidal voltage are assumed to be given along with the operating frequency as well as the passive component parameters such as load impedance and tuning inductance. The unknowns, A_d and φ_d, cannot be solved without knowing G_n. Thus, $A_d(0)$ and $\varphi_d(0)$ as well as $G_n(0)$ are initialized before the transient analysis starts. Strictly speaking, within one RF period A_d and φ_d have numerous instantaneous values, which lead to numerous corresponding instantaneous G_n values. The computer simulations could be very tedious if the detailed instantaneous solutions were tried. In this work, we adopt a new approach, which employs a generalized admittance (or impedance) to simplify simulations. The generalized admittance is defined in such a way that the device admittance remains the same within one RF period, and evaluated only at the end of one RF period. In fact, this

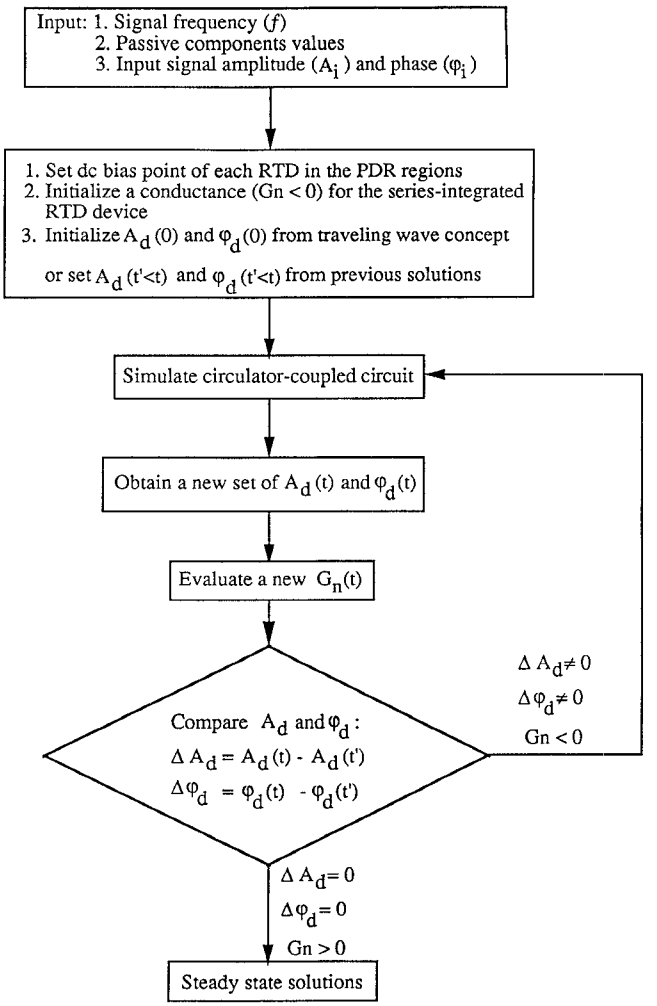

Fig. 2. A flow chart of simulation algorithm for nonlinear interaction between device and circuit.

is a good approximation, because it is the average device admittance seen by the incident wave.

During simulation process, an instantaneous new set of A_d and φ_d is obtained at the end of every RF period, and used to evaluate a new device admittance at this instant. This new instantaneous device admittance will then be used to determine A_d and φ_d of the next RF period. The subsequent circuit and device behaviors can thus be determined. The simulation process will repeat one after the other RF period until the stabilized steady state is reached. When this happens, the dc bias point of every RTD should have been pulled into the NDR region. If the amplitude of the input sinusoidal voltage is not adequate, a stable operation mode will not occur. Then, a new input power level, which is related to load conductance and initial device conductance, should be estimated and tried for the whole simulation process again. The simulation results under various conditions can guide us to an optimum design of the circulator-coupled series-integrated quantum-well RTD oscillator.

IV. Analytical Solution

The numerical simulation process seems very complicated. Nevertheless, it is possible to get an analytical solution un-

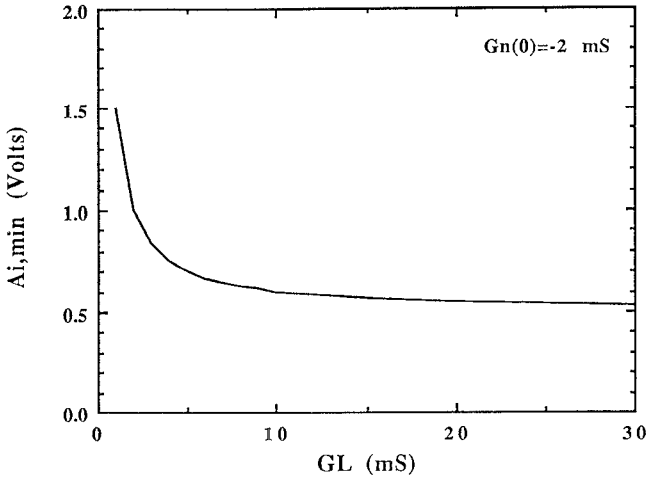

Fig. 3. Minimum input voltage amplitude (Ai) versus load conductance (GL) for a two-RTD device in the circulator-coupled circuit.

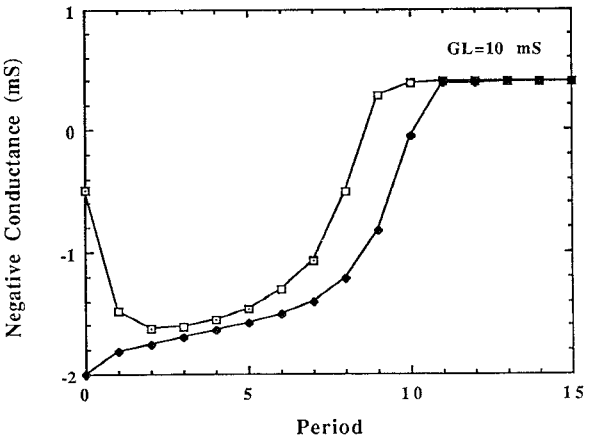

Fig. 4. Conductance transient response of a two-RTD device in the circulator-coupled circuit of 100 GHz with two different initial device conductance ($Gn(0)$). One period is 10 ps.

der certain circumstances. Assume that the phase difference between φ_i and φ_d is very small, so (18) becomes

$$\varphi_d = (\omega - \omega_o)t + \varphi_d(0) \tag{20}$$

where $\varphi_d(0)$ is the initial φ_d. If ω is very close to ω_o, the phase variation of φ_d with time is negligible. Let us assume that G_n is a constant. Then (17) simplifies to

$$dA_d/dt + A_d/T = K \tag{21}$$

where $T = 2C_j/(G_L - G_n)$, and $K = G_L A_i/C_j$. The solution to (21) can be realized as

$$A_d(t) = KT - (KT - A_d(0))e^{-t/T} \tag{22}$$

where $A_d(0)$ is the initial A_d. A_d at final steady state should be

$$A_d(T_f) = 2G_L A_i/(G_L - G_n(T_f)) \tag{23}$$

where $G_n(T_f)$ is the device conductance at final steady state. The initial $A_d(0)$ in the simulations can be estimated using (23) by simply replacing $G_n(T_f)$ with its initial value $G_n(0)$.

In order to effectively relocate dc bias point of each individual RTD in the series-integrated device from PDR regions to NDR region, A_d must be greater than V_t all the time [11]. Therefore, from (23) the minimum input voltage amplitude should be

$$A_{i,\min} \geq V_t(G_L - G_n(0))/(2G_L) \tag{24}$$

Apparently, A_i strongly depends on the initial device conductance and load conductance.

V. Simulation Results

We chose a GaAs/AlAs quantum-well RTD from wafer 3 in [12] in our simulations. $G_n(0)$ is estimated to be equal to -2 mS for a two-RTD device. The minimum A_i versus G_L for a two-RTD device is plotted in Fig. 3. A smaller G_L requires a larger A_i to begin with in order to get into a stable operation mode. However, the resulting larger A_d may produce a positive stable device conductance generating no oscillations when the steady state is reached.

The conductance transient response of a two-RTD device in the circulator-coupled circuit at 100 GHz is shown in Fig. 4, where one period is 10 ps. Two cases with different initial positive device conductance are simulated. One starts $G_n(0)$ with -2 mS, while the other with -0.5 mS. All the initial simulation conditions remain the same for these two cases. (i.e., $A_i = 0.6$ V, $\varphi_i = 0, A_d(0) = 1.0$ V, $\varphi_d(0) = 0, G_L = 10$ mS, $V_{\rm dc} = 1.95$ V, $V_{\rm dc1} = 1.6$ V, and $V_{\rm dc2} = 0.35$ V.) The curve starting with $G_n(0)$ of -2 mS has a smooth transition to reach steady state. Although initial G_n of -0.5 mS seems off, the corresponding response curve will quickly adjust itself to follow the right track to reach steady state. This indicates that the initial G_n value used in the simulation is not critical to the final solution as long as A_i is appropriate. Indeed, A_i is found to be the most critical parameter. If A_i is less than the minimum value of (24), the simulations show no stable solution. In this work, the operating frequency is chosen so close to the resonance frequency that the phase change of the total RF voltage across the device is less than 0.1 degree, which is not significant at all. It is also noticed that a smaller initial value of $|G_n|$ can lead to a faster convergence rate due to a corresponding larger A_d obtained in the simulation process. When dc bias point of each individual RTD is moved closer to NDR region during simulation, the convergence rate becomes even faster.

The role of the load conductance in the two-RTD circuit is also investigated. The results are presented in Fig. 5, where two different load conductances (20 mS and 10 mS) are simulated. The initial conditions are identical for both cases. As shown in Fig. 5, a larger G_L value results in a higher negative device conductance due to a smaller A_d at the final steady state. Notice that the convergence rate in Fig. 5 is faster than that in Fig. 4. This is because dc bias points in Fig. 5 are intentionally moved closer to the NDR region of the I-V characteristics ($V_{\rm dc1} = 1.5$ V, and $V_{\rm dc2} = 0.45$ V).

The conductance of the two-RTD device in the circulator-coupled circuit versus the amplitude of the RF voltage across the device is plotted in Fig. 6, where steady-state and transient curves are shown. The solid curves resulting from the stable steady-state solutions have been analyzed in [5]. The dotted

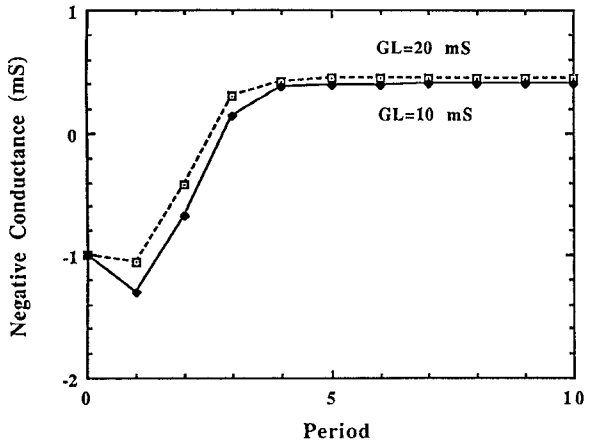

Fig. 5. Conductance transient response of a two-RTD device in the circulator-coupled circuit of 100 GHz with two different load conductance (G_L). One period is 10 ps.

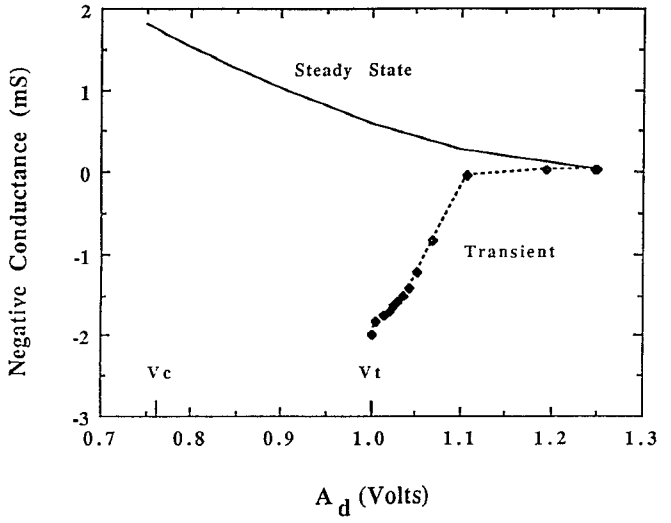

(a)

Fig. 6. Conductance of a two-RTD device in the circulator-coupled circuit versus the amplitude of the RF voltage across the device. Solid curve is for steady state, while dotted one is for transient. V_c and V_t are cutoff and threshold voltages, respectively. (a) G_L is 10 mS, and A_i is 0.6 V.

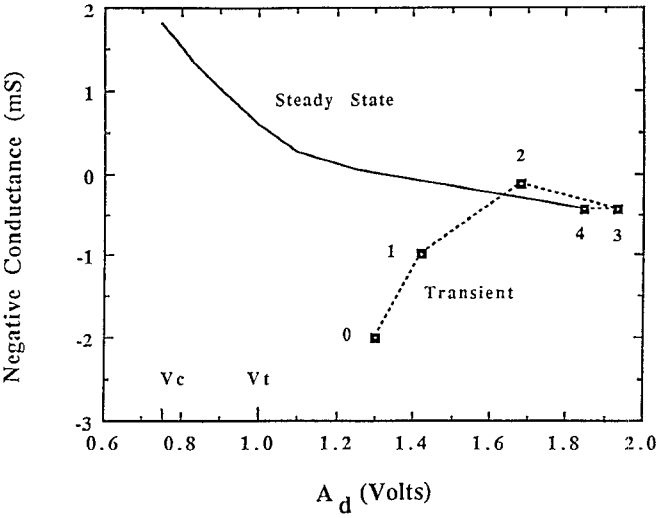

(b)

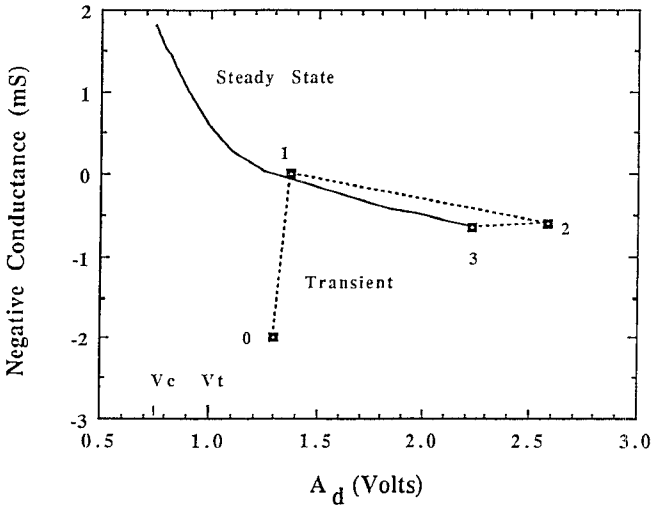

(c)

Fig. 6. (continued) (b) G_L is 5 mS, and A_i is 1.2 V, (c) G_L is 1.5 mS, and A_i is 1.6 V.

curves display the simulated transient behavior under various conditions. V_c and V_t are also marked in Fig. 6.

The dotted curve in Fig. 6(a) starts with $G_n(0)$ of -2 mS at $A_d(0) = 1$ V under the condition of $G_L = 10$ mS and $A_i = 0.6$ V. The transient interaction between device and circuit prompts A_d to increase so that dc bias point on each RTD will be pulled towards the NDR region of the I–V characteristics, leading to a less positive device conductance. The small positive conductance will in turn further increase A_d, which pulls dc bias point further close to NDR region. The conductance transient process is clearly displayed by the dark spots on the transient curve, where each dark spot represents the simulation result at the end of one RF period. At the very beginning, the movement of A_d and G_n is very slow due to a small differential between V_d and V_t. As time goes on, the difference between V_d and V_t increases so that G_n becomes closer to its steady-state curve. This iterative interaction process will continue and eventually put the dc bias point of each RTD inside the NDR region. It takes about 13 RF periods to reach the steady-state solution. When the final steady state is achieved, as shown in Fig. 6(a) the transient curve terminates on the steady-state curve, where G_n has a value of 0.04 mS at $A_d = 1.25$ V. At this moment G_n is far away from its maximum available value, and the circuit is in an amplifier mode. A_i can be reduced in order to optimize G_n. During the process of decreasing A_i, dc bias point of each RTD remains inside the NDR region of its I–V characteristics as long as $A_d(t)$ is greater than V_c. It is found that the device conductance closely follows the steady-state curve to reach its optimum value after A_i is reduced.

If load conductance is chosen to be closer to or smaller than the absolute value of the maximum stable negative conductance ($|G_{n,\max}|$), a higher A_i is required to initiate the circuit. This results in a quite different conductance transient curve. For example, G_L is changed from 10 mS to 5 mS, the simulation result is shown in Fig. 6(b), where A_i is set at 1.2 V. The transient curve starts at $G_n(0) = -2$ mS and $A_d(0) = 1.3$ V. The numbers next to dark spots of the transient curve represent RF periods. Because A_i is large, A_d is quickly adjusted to a large magnitude to pull bias point of each RTD

into the NDR region. G_n increases with time until the second period. At the end of second period, the dc bias points are just moved into NDR region and G_n overshoots the steady-state curve. G_n is then pulled down during the third period, and reaches the steady-state point at the end of fourth period. It is worthwhile to point out that a large A_i or a high input power assures a fast convergence.

If G_L is further reduced to 1.5 mS, which is less than $|G_{n,\max}|$, the simulation result is shown in Fig. 6(c). The steady-state point is reached at the end of third period. If input power is suddenly shut off at this moment, an oscillator mode occurs at $G_L = |G_n| = 1.5$ mS with output power of 0.5 mW. The pulse width of the input pulsed power required to initiate the oscillations depends on the load conductance. As indicated in Figs. 6(b) and 6(c), the pulse width is no longer than 5 periods (e.g., equivalent to 50 ps at oscillation frequency of 100 GHz), if load conductance is set very close to $|G_{n,\max}|$.

In fact, the maximum oscillation output power occurs at $G_L = |G_{n,\max}|$. Therefore, the maximum output power versus the minimum input power ratio (p) can be expressed as

$$p = P_{\text{out},\max}/P_{\text{in},\min} = \{(V_c/V_t)[2G_{n,\max}/(|G_n(0)| + G_{n,\max})]\}^2 \quad (25)$$

Based on the experimental quantum-well RTD I-V curve in [12], $|G_n(0)|$ is approximately equal to $G_{n,\max}$. Equation (25) thus becomes a simpler form as

$$p \approx (V_c/V_t)^2 \quad (26)$$

The ratio is estimated to be better than 50% in this work. This result is very encouraging, because half of the high pulsed power from IMPATT can be converted to CW power at millimeter-wave frequencies.

VI. Conclusion

In light of the newly developed pulsed IMPATT, a novel RF initiation scheme to generate millimeter-wave oscillations in the series-integrated quantum-well RTD's is proposed and analyzed for the first time. A reflection-type circuitry employing a circulator is investigated. The simulations of a two-RTD circuit at 100 GHz indicate that it is possible to convert a pulsed power into a CW power through the circuit oscillation mode. The input pulsed power, for example, can be provided by the pulsed IMPATT operated in a very short pulse width of 50 ns or less. The power conversion rate of maximum output power versus minimum input power is estimated as high as 50%. These interesting results will provide a practical application for the series-integrated quantum-well RTD and the new pulsed IMPATT.

References

[1] V. P. Kesan, A. Mortazawi, D. R. Miller, V. K. Reddy, D. P. Neikirk, and T. Itoh, "Microwave and millimeter-wave QWITT diode oscillators," *IEEE Trans. Microwave Theory Tech.*, vol. MTT-37, pp. 1933–1941, Dec. 1989.

[2] H. Gronqvist, A. Rydberg, H. Hjelmgren, H. Zirath, E. Kollerg, J. Soderstrom, and T. Anderson, "A millimeter wave quantum well diode oscillator," in *Proc., 18th Euro. Microwave Conf.*, Stockholm, Sweden, Sept. 1988, pp. 370–375.

[3] E. R. Brown, J. R. Soderstrom, C. D. Parker, L. J. Mahoney, K. M. Molvar, and T. C. McGill, "Oscillations up to 712 GHz in InAs/AlSb resonant-tunneling-diodes," *Appl. Phys. Lett.*, vol. 58, pp. 2291–2293, May 1991.

[4] Y. I. Vorontsov and I. V. Polyakov, "Study of oscillatory processes in circuits with several series-connected tunnel diodes," *Radio Eng. Electron. Phys.*, vol. 10, pp. 758–763, May 1965.

[5] C. C. Yang and D. S. Pan, "Theoretical investigations of a proposed series integration of resonant tunneling diodes for millimeter-wave power generation," *IEEE Trans. Microwave Theory Tech.*, vol. MTT-40, pp. 434–441, Mar. 1992.

[6] C. J. Madden, R. A. Marsland, M. J. M. Rodwell, D. M. Bloom, and Y. C. Pao, "Hyperabrupt-doped GaAs nonlinear transmission line for picosecond shock-wave generation," *Appl. Phys. Lett.*, vol. 54, pp. 1019–1021, Mar. 1989.

[7] P. A. Rolland, C. Dalle, and M. R. Friscourt, "Physical understanding and optimum design of high-power millimeter-wave pulsed IMPATT diodes," *IEEE Electron Device Lett.*, vol. 12, pp. 221–223, May 1991.

[8] I. Song and D. S. Pan, "Analysis and simulation of the quantum well injection transit time diode," *IEEE Trans. Electron Devices*, vol. 35, pp. 2315–2322, Dec. 1988.

[9] K. Kurokawa, "Some basic characteristics of broadband negative resistance oscillator circuits," *Bell Syst. Tech. J.*, vol. 48, pp. 1937–1955, July-Aug. 1969.

[10] H. J. Kuno, "Analysis of nonlinear characteristics and transient response of IMPATT amplifiers," *IEEE Trans. Microwave Theory Tech.*, vol. MTT-21, pp. 694–702, Nov. 1973.

[11] C. C. Yang, "Theoretical investigations of a proposed series integration of resonant tunneling diodes for millimeter-wave power generation," Ph.D. dissertation, University of California, Los Angeles, CA, 1991.

[12] E. R. Brown, T. C. L. G. Sollner, W. D. Goodhue, and C. D. Parker, "Millimeter-band oscillations based on resonant tunneling in a double-barrier diode at room temperature," *Appl. Phys. Lett.*, vol. 50 , pp. 83–85, Jan. 1987.

[13] C. C. Yang and D. S. Pan, "Millimeter-wave simulation of a series-integrated resonant tunneling diode including transit time effect," *MTT-S Int. Microwave Symp.*, Atlanta, GA, pp. 329–332, June 1993.

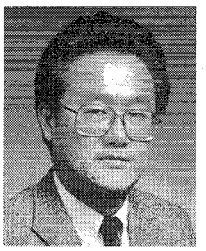

Cheng Chih Yang (S'82, M'84) was born in Taiwan, China, in 1955. He received the B.S. degree in physics from National Cheng Kung University, Tainan, Taiwan, in 1977, and the M.S., Engineer, and Ph.D. degrees in electrical engineering from the University of California, Los Angeles.

From 1977 to 1979 he served as an infantry platoon leader in Chinese Army. From 1979 to 1983 he was a research and teaching assistant at UCLA, where he conducted research in the area of microwave electronics. In 1983, he joined Commodore MOS Technology, Costa Mesa, CA, where he worked on SPICE modeling and CMOS logic circuits. In 1984, he joined Electronic Systems Group of TRW Inc., Redondo Beach, CA, where he has been an IR&D principal investigator and a project manager responsible for developing microwave and millimeter-wave circuits and subsystems, such as low-noise amplifiers, mixers, multipliers, downconverters, detectors, and frequency synthesizers. Currently, he is responsible for the development of millimeter-wave low-noise amplifiers for satellite communication systems. He is also developing millimeter-wave phased array electronics and packaging for advanced technology programs. His interests include device characterization and modeling, microwave and millimeter-wave integrated circuits design, and communication system hardware development.

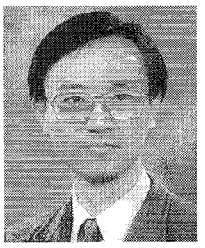

Dee-Son Pan (M'89) received the B.S. degree in physics from Tsing-Hwa University, Taiwan, China, in 1971, and the Ph.D. degree in physics from the California Institute of Technology in 1978.

He joined the faculty of the Electrical Engineering Department at the University of California, Los Angeles, as an assistant professor in 1977, where he is currently an associate professor. His current research interests are device modeling, semiconductor physics, and theoretical exploration of new devices.